Progress In Electromagnetics Research B, Vol. 97, 1–18, 2022

Robust Multi-Objective Optimization for BEESM Based on Improved Climbing Algorithm

Naxi Xu[1], Xiaodong Sun[1, *], Ke Li[2], and Ming Yao[3, *]

Abstract—Robust optimization design of brushless electrically excited synchronous machines (BEESMs) is a problem that has received extensive attention. The increase in finite element calculation cost due to the increase in the number of motor parameters is one of the main problems faced by optimization. In this paper, a robust multi-objective optimization design method of BEESM based on an improved hill-climbing algorithm is proposed. All design parameters are divided into three subspaces according to the sensitivity by the sensitivity analysis method combined with Kendall's rank coefficient, thereby reducing the consumption required for finite element model (FEM) calculation. The screening problem of Pareto frontier solutions is solved by an improved hill-climbing algorithm. The candidate points to be optimized are screened through the improved climbing algorithm, and only the candidate points located on the Pareto frontier will be optimized, which ensures the high performance of the candidate points. Based on the noise problems that may occur in actual production and processing, the candidate points are robustly analyzed, and the optimal design is screened out. The robust optimization design method proposed in this paper can reduce the computational cost and improve the robustness of the motor based on improving the performance of the motor.

1. INTRODUCTION

Because of its high power factor and adjustable power factor, brushless electrically excited synchronous machine (BEESM) is widely used in motoring and power generation [1–3]. For example, high-power hoists, large-capacity rolling mills, fans, pumps, and compressors all use electric excitation synchronous motor drive systems. Therefore, the research on BEESM is a hot issue in recent years [4–6].

The development and optimization of the motor topology are the two main aspects to improve the overall performance of the BEESM [7–11]. Zhang et al. proposed a novel BEESM with a hybrid rotor. This motor has two windings with different numbers of poles to provide excitation and drive torque independently [12]. Long et al. proposed a new BEESM with an arc-shaped rotor structure. The armature and field windings of this motor are placed on the stator [13]. Ali et al. proposed a new BEESM based on the generation and utilization of a subharmonic component of the stator magnetomotive force [14]. Yao et al. presented a BEESM with a distinctive rotor structure and additional harmonic field windings [15]. Spielmann and Friedrich investigated the effect of increasing skew on reducing torque and increasing excitation independent ripple. However, when it comes to a wide application in the industrial field, existing structures may not be suitable because the actual fabrication process has not been studied. Therefore, the robust design of BEESM is necessary [16].

On an optimization problem for electrical equipment, studies usually try to find the global optimal solution of the objective function [17–20]. However, these optimal solutions may exhibit unsatisfactory

Received 9 August 2022, Accepted 16 September 2022, Scheduled 10 October 2022

* Corresponding author: Xiaodong Sun (xdsun@ujs.edu.cn), Ming Yao (ymluck@ujs.edu.cn).

[1] Automotive Engineering Research Institute, Jiangsu University, Zhenjiang 212013, China. [2] School of Electrical and Information Engineering, Jiangsu University, Zhenjiang 212013, China. [3] School of Automotive and Traffic Engineering, Jiangsu University, Zhenjiang 212013, China.

performance when uncertainties in the production process are taken into account [21–24]. Many studies try to solve optimization problems with uncertainty, but there are still some problems in current research. First, as design parameters continue to increase, the cost of FEM computation will rapidly increase, resulting in unacceptable computational costs [25–28]. The corresponding solution is the combination of a multi-objective intelligent optimization algorithm and surrogate model. With the continuous development of optimization algorithms, more and more multi-objective intelligent optimization algorithms, such as genetic algorithm (GA), particle swarm optimization (PSO), and differential evolution algorithm (DEA), are used in the optimization of electrical equipment [29–33]. Also, the development of surrogate model technology has greatly contributed to the reduction of FEM computation time [34]. However, since the establishment of the surrogate model also needs the support of FEM calculation, when the optimization parameters increase, the industry of the surrogate model encounters a bottleneck. Another problem is finding the robust optimal solution [35–38]. Since the multi-objective optimization algorithm obtains a Pareto front including a series of solution sets, finding a method that can obtain a robust solution with high performance has become one of the main problems of a robust design.

To solve the above problems, this paper proposes a BEESM robust multi-objective optimization design method based on an improved climbing algorithm. All design parameters are divided into three subspaces according to the sensitivity by the sensitivity analysis method combined with Kendall's rank coefficient, thereby reducing the consumption required for FEM calculation. The screening problem of Pareto frontier solutions is solved by an improved climbing algorithm. The candidate points to be optimized are screened through the improved climbing algorithm, and only the candidate points located on the Pareto frontier will be optimized, which ensures the high performance of the candidate points. Based on the noise problems that may occur in actual production and processing, the candidate points are robustly analyzed, and the optimal design is screened out.

The rest of this paper is organized as follows. Section 2 introduces the robust multi-objective optimization method proposed in this paper. Section 3 introduces the principles of robust optimization methods. Starting from Section 4, we take a BEESM as an example to implement the robust multi-objective optimization method proposed in this paper. Section 5 presents the results of sensitivity analysis and parameter stratification. Section 6 presents the optimization results of the motor and analyzes the results, followed by the conclusion.

2. MULTI-OBJECTIVE OPTIMIZATION METHOD

2.1. Over View of Optimization Methods

Traditional BEESM optimization methods often choose to optimize all design parameters in the same space, and such optimization methods will lead to a lot of computational consumption. To reduce the consumption of FEM calculation in the optimization process, a surrogate model is usually used as an approximate model of FEM. However, as the design parameters increase, the computational cost of FEM required to train the surrogate model increases exponentially. Therefore, to solve the problem of the increase of FEM calculation consumption caused by the increase of design parameters, all design parameters are divided into three subspaces and optimized respectively according to the results of sensitivity analysis.

During the production and processing of the motor, due to the limitation of production conditions, there will inevitably be a certain error between the size of the machined motor and the size of the design. The error brought by the machining will lead to a big difference in the design performance of the machined prototype and the motor. Therefore, the robust design of the motor is very necessary. In the optimization process of each subspace, the robust optimization design of the motor is carried out to avoid the degradation of motor performance caused by motor processing errors to the greatest extent.

As shown in Figure 1, the robust multi-objective optimization design flow of BEESM is divided into two parts: preprocessing and multi-layer optimization.

The purpose of the preprocessing part is to establish the mathematical model of the optimization problem and preprocess the design parameters before the multi-objective optimization of BEESM. The main steps of this part are as follows.

Step1: Initial design

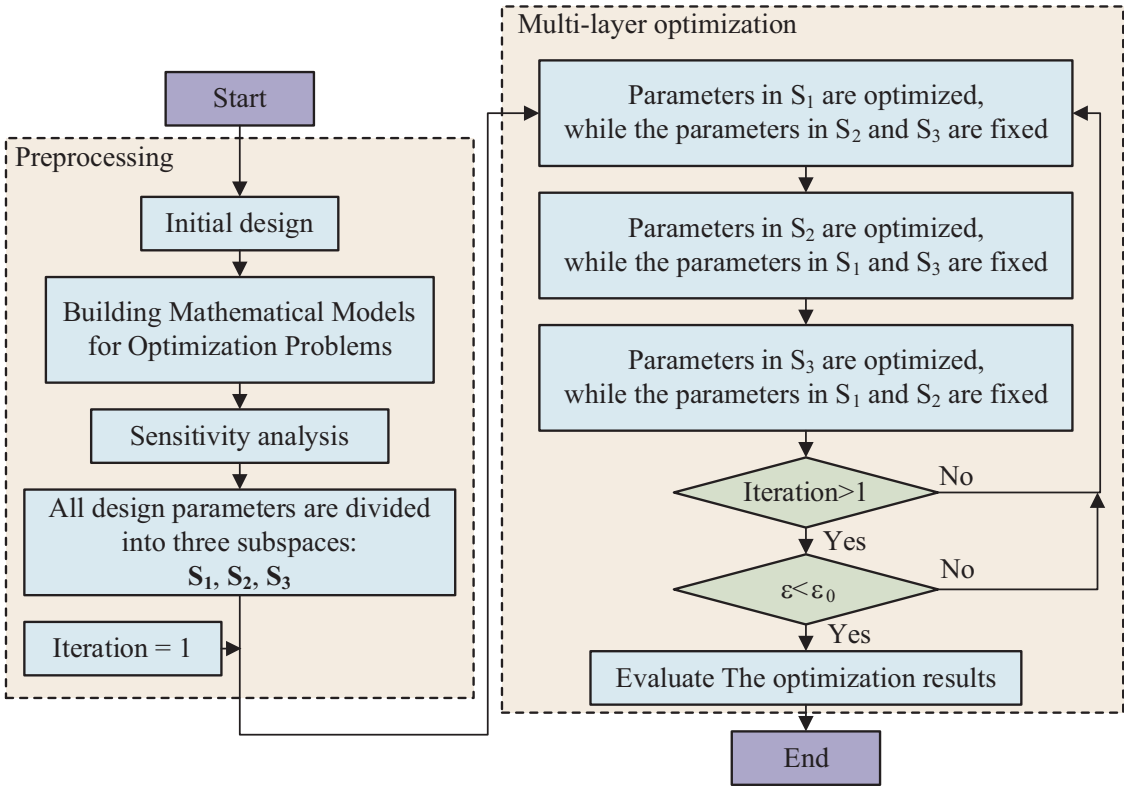

Figure 1. Optimization design flow chart.

First, determine the design requirements of BEESM according to the actual situation. Determine the initial design parameters of the motor according to different motor design requirements.

Step2: Building Mathematical Models for Optimization Problems

The second step is to determine the optimization problem of BEESM and convert the optimization problem into a mathematical model. In this step, it is necessary to first determine which design parameters of the motor need to be optimized and determine the optimization range of these design parameters. An unreasonable optimization range will result in the motor not being able to find the optimal design through optimization, or the designed motor will not be used normally. At the same time, different design parameters may form a closed dimensional chain, or there is a constraint relationship, and the relationship between these design parameters also needs to be considered. Second, for different design problems, determine the goal of motor optimization. There are many indicators for evaluating motor performance, such as rated torque, torque ripple, efficiency, and loss. There is a positive correlation between some indicators, while other indicators are difficult to find the optimal design at the same time. In addition, different motor design problems also put forward different requirements for these indicators. Therefore, it is necessary to determine the optimization goal of the motor according to the specific motor design problem.

Step3: Sensitivity analysis

Different optimization objectives tend to have different sensitivities to different design parameters. If all design parameters are optimized equally without considering the sensitivity of design parameters, the optimization cost will increase. In addition, since the same optimization method is used for sensitive and non-sensitive parameters, the design parameters that are sensitive to the optimization objective may not be optimized to find the best design. Therefore, this paper proposes a sensitivity analysis method that combines Kendall's rank coefficient and local sensitivity analysis. The sensitivity of the design parameters is evaluated by the sensitivity analysis method proposed in this paper and used as the basis for the space division of the design parameters in the next step.

Step4: All design parameters are divided into three subspaces: $\mathbf{S}_1$, $\mathbf{S}_2$, $\mathbf{S}_3$

To improve the efficiency of motor optimization, all parameters are divided into three subspaces based on the sensitivity standard. These three subspaces are composed of parameters with different levels of sensitivity: high-sensitivity parameters $\mathbf{S}_1$, sensitive parameters $\mathbf{S}_2$, and non-sensitive parameters. parameter $\mathbf{S}_3$.

The above four steps constitute the preprocessing part. Through the previous four steps, the optimization problem of the motor is transformed into a mathematical model, and all design parameters are divided into three subspaces according to the results of sensitivity analysis. The design parameters of the next three subspaces will be designed for robust optimization respectively.

The purpose of the multi-layer optimization part is to optimize the parameters of the partitioned space in order and evaluate the results obtained by the optimization. The main steps of this part are as follows:

Step1: Parameters in $\mathbf{S}_1$ are optimized, while the parameters in $\mathbf{S}_2$ and $\mathbf{S}_3$ are fixed

Since the design parameters in $\mathbf{S}_1$ are more sensitive to the optimization objective, the design parameters in this space are optimized in the first step. In this step, the design parameters in $\mathbf{S}_2$ and $\mathbf{S}_3$ are fixed as initial values, and the design parameters in $\mathbf{S}_1$ are optimized separately. Through the optimization of the robust multi-objective design method of the motor based on the Climbing algorithm, the optimal design point that meets the motor design conditions is found. The optimized design parameters in subspace $\mathbf{S}_1$ will be input into the next step.

Step2: Parameters in $\mathbf{S}_2$ are optimized, while the parameters in $\mathbf{S}_1$ and $\mathbf{S}_3$ are fixed

The optimization process for this step is similar to the previous step. After the high sensitivity parameters are optimized, the sensitive parameters will be optimized. In this step, the design parameters in $\mathbf{S}_1$ are fixed to the results obtained by the optimization in the previous step; the design parameters in $\mathbf{S}_3$ are fixed as the initial values; and the design parameters in $\mathbf{S}_2$ will be optimized. The result will be output to the next step.

Step3: Parameters in $\mathbf{S}_3$ are optimized, while the parameters in $\mathbf{S}_1$ and $\mathbf{S}_2$ are fixed

Since the design parameters in $\mathbf{S}_3$ are the least sensitive to the optimization objective, the design parameters in this part are placed at the end for optimization. Similarly, the design parameters in $\mathbf{S}_1$ are fixed to the results obtained through Step1 optimization; the design parameters in $\mathbf{S}_2$ are fixed to the results obtained through Step2 optimization; and the design parameters in $\mathbf{S}_3$ are optimized. After the design parameters in $\mathbf{S}_3$ are optimized, all design parameters in the design space are optimized. The optimization results of all design parameters will be output to the next step.

Step4: Determine whether the convergence conditions are met, and if the convergence conditions are met, stop the optimization and output the results. If the convergence conditions are not met, the optimization of the design parameters continues until the convergence conditions are met.

Through the above three steps, all design parameters are preliminarily optimized. To ensure that the optimization result does not fall into a local optimal solution, an optimization iteration consisting of steps 1–3 will loop continuously. In this step, first, determine whether the number of current iterations is greater than 1. If the current iteration is the first time, go directly to the next iteration process. If the number of iterations experienced by the current optimization exceeds 1, continue to judge whether the convergence condition is satisfied. The condition for convergence is whether the optimization produced by the current iteration process is less than the given error, where ε_0 is the given error, and the error generated by the current iteration process can be calculated by:

$$\varepsilon = \max\left\{\frac{|f_1(x_i) - f_1(x_{i-1})|}{f_1(x_{i-1})}, \frac{|f_2(x_i) - f_2(x_{i-1})|}{f_2(x_{i-1})}, \ldots, \frac{|f_j(x_i) - f_j(x_{i-1})|}{f_j(x_{i-1})}\right\} \tag{1}$$

where f is the optimization objective, x_i the current design parameter space, and x_{i-1} the design parameter space generated by the previous iteration process.

2.2. Build Mathematical Models

The purpose of the initial design is to determine the design requirements of the BEESM according to the actual situation and to determine the initial design parameters of the motor for different motor design requirements. After the initial design is completed, it is necessary to determine the parameters of the motor that need to be optimized according to the motor structure obtained from the initial design, and

determine the target to be optimized according to the design requirements. The optimization objective of the motor is defined as:

$$\min : \begin{cases} f_1(\mathbf{x}) \\ f_2(\mathbf{x}) \\ \vdots \\ f_j(\mathbf{x}) \end{cases} \tag{2}$$

where $\mathbf{x}$ is the design space composed of all design parameters and

$$\mathbf{x}_{\min} \leq \mathbf{x} \leq \mathbf{x}_{\max} \tag{3}$$

where $\mathbf{x}_{\min}$ is the lower bound of the design parameters, and $\mathbf{x}_{\max}$ is the upper bound of the design parameters. In addition to the constraints imposed by the upper and lower boundaries of the design parameters on the design parameters, there may be constraints between different design parameters, which can be expressed as:

$$\begin{cases} g_1(\mathbf{x}) \leq 0 \\ g_2(\mathbf{x}) \leq 0 \\ \vdots \\ g_m(\mathbf{x}) \leq 0 \end{cases} \tag{4}$$

2.3. Sensitivity Analysis

To divide the design parameters into different design spaces, it is necessary to judge the influence degree of different design parameters on the optimization objective. Therefore, a sensitivity analysis of the design parameters is necessary. Three correlation analysis methods, Pearson, Spearman, and Kendall, are usually used to judge correlation. Due to the equidistant orthogonal experimental design and the Kendall coefficient having better performance in many cases, the Kendall correlation coefficient was selected to be used in this sensitivity analysis [39]. The Kendall rank correlation coefficient can be defined as:

$$K = \frac{c - d}{\sqrt{\left(\frac{1}{2}N(N-1) - \sum \frac{t_i(t_i-1)}{2}\right)\left(\frac{1}{2}N(N-1) - \sum \frac{u_i(u_i-1)}{2}\right)}} \tag{5}$$

where c is the number of pairs in the same order, d the number of pairs in the opposite order, N the number of experiments, and t_i, u_i are the design parameters and the number of elements contained in the ith small set in the optimization objective, respectively. Since there is often a nonlinear relationship between the design parameters of the BEESM and the optimization objective, the Kendall coefficient can help determine sensitivity. The value of the Kendall correlation coefficient ranges from -1 to 1. The closer the absolute value of the Kendall correlation coefficient is to 1, the greater the correlation is between the two variables, and the closer it is to 0, the smaller the correlation is between the two variables. A positive or negative Kendall coefficient indicates whether the relationship between two variables is positive or negative. Local sensitivity can be defined as:

$$S = \left| \frac{\left(f\left(\mathbf{x}_0 \pm \Delta\mathbf{x}_i\right) - f\left(\mathbf{x}_0\right)\right)/f\left(\mathbf{x}_0\right)}{\pm\Delta\mathbf{x}_i/\mathbf{x}_0} \right| \tag{6}$$

where $\Delta\mathbf{x}_i$ is the variation of the design parameters, and $\mathbf{x}_0$ is the initial design value of the design parameters. In this paper, Kendall coefficients are used to judge the nonlinear relationship between motor design parameters and optimization objectives. The final sensitivity calculation method is:

$$P = |K * S| \tag{7}$$

2.4. Subspace Optimization

The optimization of each subspace has a similar process. As shown in Figure 2, a full factorial experimental design was firstly performed based on the design parameters in $\mathbf{S}_1$. The purpose of the full factorial experimental design is to better cover the design space and ensure the accuracy of the surrogate

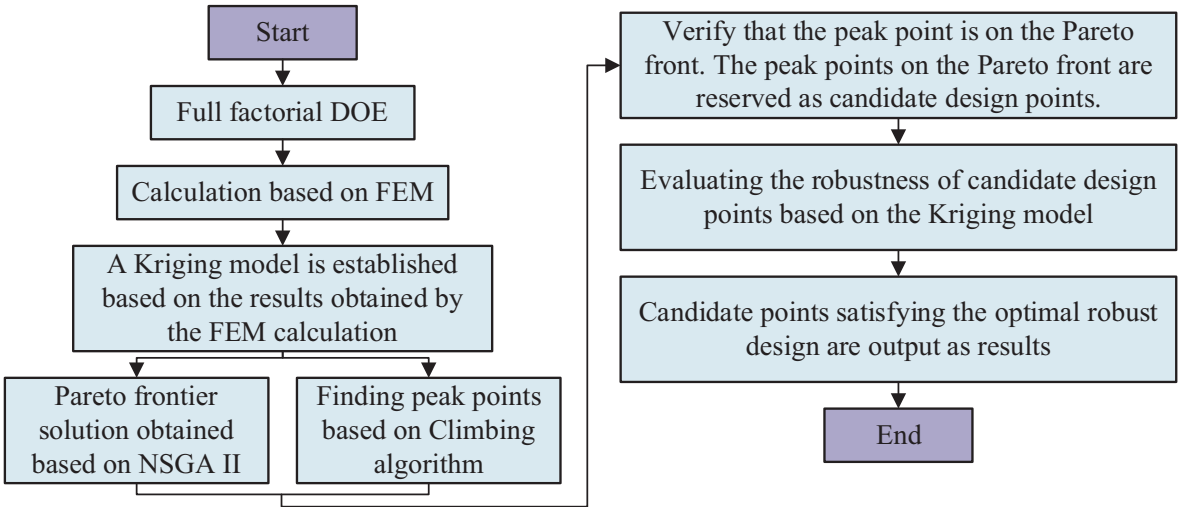

Figure 2. Subspace optimization flowchart.

model. The corresponding test results will be calculated by FEM. To improve the optimization efficiency, a surrogate model is introduced into the optimization process. This paper uses the Kriging model to build a suitable proxy model. The Kriging model is a semi-parametric model whose response value contains a mean trend term and a variance term [40]. The Kriging model has significant advantages in nonlinear modeling and has been widely used in the field of electrical design. The results obtained through the experimental design and FEM calculations will be used as training data for the Kriging model. The trained Kriging model will be used as a substitute for FEM in the next optimization process.

The next optimization will be carried out from two aspects. Due to the mutual constraints between different optimization objectives, it is impossible to optimize the design parameters of the motor to obtain the optimal solution for all the optimization objectives at the same time. The final optimization result is often a compromise among all optimization objectives. Usually, people call the solution set composed of all solutions in the design space that do not have other solutions superior to the current solution as Pareto frontier solutions. NSGA II is a multi-objective optimization algorithm and is widely used in electrical equipment optimization problems [41–43]. In this paper, NSGA II is used as a multi-objective intelligent optimization algorithm to obtain the Pareto frontier solution set of the motor. On the other hand, the peak points in the motor design space will be obtained by an improved climbing algorithm. These peaks will be verified to be on the Pareto front.

To ensure the efficient use of motor resources, only design points on the Pareto frontier will be retained. These reserved design points will be evaluated for their robustness, and the design points that satisfy the optimal robust design will be output as the result.

3. ROBUST OPTIMIZATION METHODS

3.1. Robust Optimization

The design point of the motor mentioned in the previous section will be evaluated for its robustness because the design point obtained by the optimization algorithm cannot guarantee that it will still have the same performance as the design value during the manufacturing process. There is always a certain error between the actual size and the design size of the motor in the actual processing process, which leads to a large deviation between the actual performance and the design performance of the motor. At the same time, since the solutions on the Pareto front have the characteristic that there are no other design points superior to the current solution, the selection and comparison of these solutions are also difficult. Therefore, inspired by the climbing algorithm, this paper analyzes the robustness of the design points based on the improved climbing algorithm to find the optimal robust design of the motor.

As shown in Figure 3, X1 and X2 are two extreme points, respectively, where X1 has better

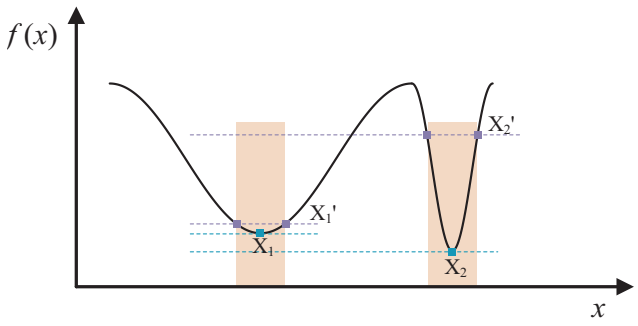

Figure 3. Solution of an optimization problem with noise problem.

performance than X2, so X1 is the local optimal solution and X2 the global optimal solution. Usually, the global optimal solution is chosen. However, when we take noise into account, things change. Since the actual design point may vary within the interval caused by noise, the local optimum has a better performance than the global optimum. So X1 may be a better choice than X2 when considering robustness issues in motor design. At the same time, the extreme points of an optimization objective include the global optimal solution and local optimal solution. These solutions may exist on the Pareto front. Find the optimal robust design of the motor by finding local peak points on the Pareto front and performing robustness analysis.

3.2. Improved Climbing Algorithm

The climbing algorithm is a local optimization method, which adopts the heuristic method and is an improvement to depth-first search. It uses the feedback information to help generate the decision of the solution, which belongs to a kind of artificial intelligence algorithm. Climbing algorithms usually start at a random point and change the position of the current point by constantly transforming. Decide whether the current change is retained or not based on how good the change is. This process of change continues until a local optimal solution is found. However, this method has the disadvantage that only an uncertain local optimal solution can be found through the climbing algorithm.

To solve this problem, an improved climbing algorithm is developed in this paper. Figure 4 is a flowchart of the improved climbing algorithm. As shown in the figure, a series of initial design points are firstly randomized, and these design points collectively constitute the set S. The results are calculated based on the Kriging model obtained through the previous training. Randomly generate new design points within a given step size, and judge whether these design points are out of bounds. Design points that are out of bounds will be discarded and regenerated until all design points are within the design bounds. The new design points together constitute the set P. Same as set S, the new design points are calculated based on the Kriging model. The design points in P and S are compared. If the design point in P is better than the design point in S, the corresponding design point is replaced. If the design point in P is not better than the design point in S, keep the design point in S and record the number of times the current design point has undergone iterations and has not been replaced. After the replacement is completed, a new design set S will be generated, and the set P will be regenerated within the given step size range. The current loop is repeated until the iteration requirements are met. Record all design points that have undergone iterations and have not been replaced a given number of times. After that, a new initial design point is randomly generated, and the previous operation is repeated until the termination requirement is met. After the algorithm is finished, all design points that satisfy the requirements will be obtained.

3.3. Robust Selection

After determining the peak points through the climbing algorithm, continue to judge whether these peak points exist on the Pareto front. To guarantee the performance of BEESM, all peak points that are not on the Pareto frontier will be discarded. To evaluate the robustness of the remaining design

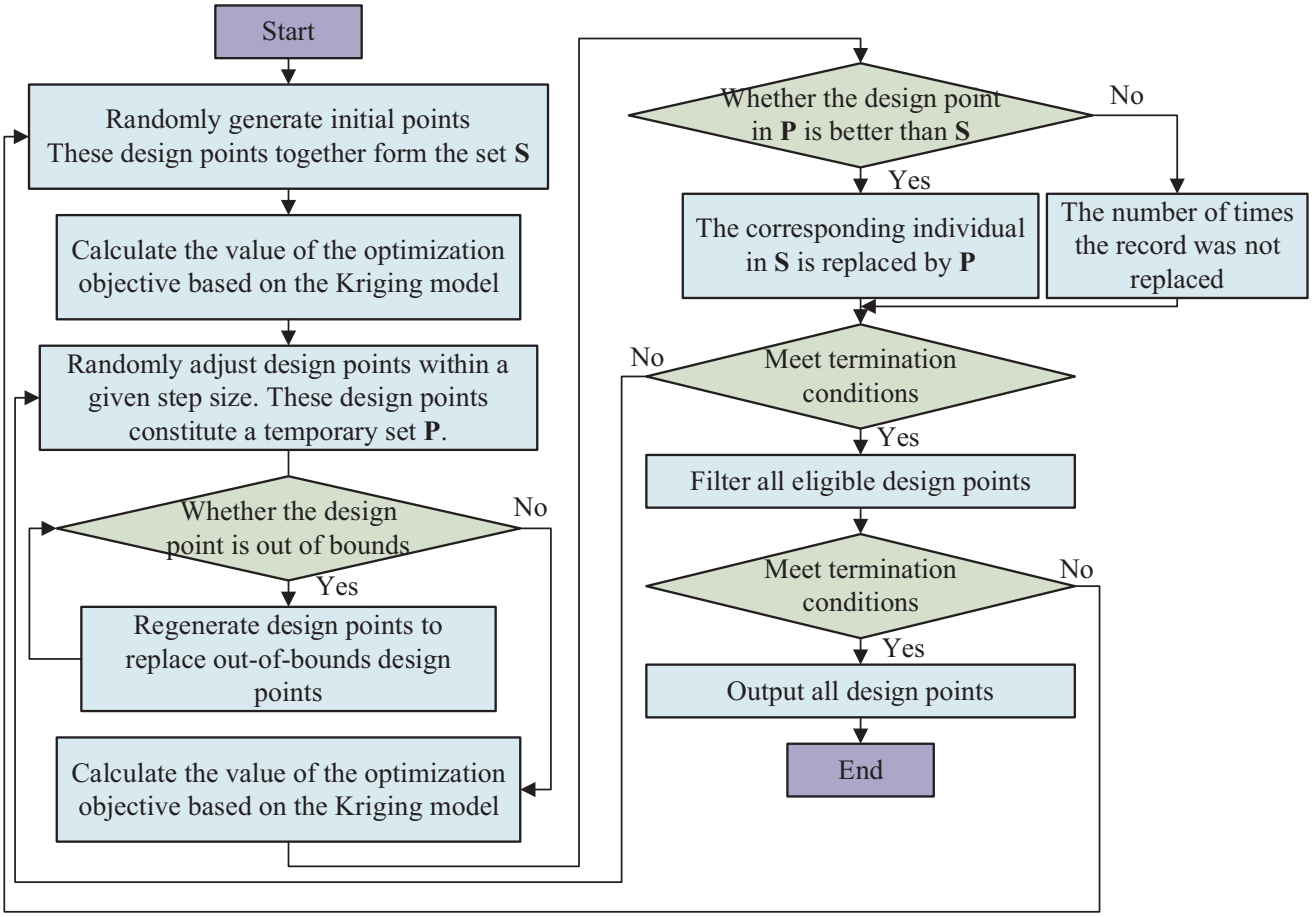

Figure 4. The flowchart of the improved Climbing Algorithm.

points, random noise based on the Kriging model will be imposed on the design points. The robustness at the design point is defined as:

$$R = \sum \omega_i \frac{f_i\left(\mathbf{x}_p + \Delta\mathbf{x}_n\right) - f_i\left(\mathbf{x}_p - \Delta\mathbf{x}_n\right)}{f_i\left(\mathbf{x}_p\right)} \tag{8}$$

where ω_i is the weight corresponding to the optimization objective, $\mathbf{x}_p$ the current design point, and ΔX_i the possible noise. The smaller the robustness value is, the better the performance of the current design point is.

4. INITIAL DESIGN AND ESTABLISHMENT OF MATHEMATICAL MODELS

Starting from this section, a robust multi-objective optimization design based on an improved climbing algorithm will be implemented based on a specific BEESM motor. Based on past research, the topology of BEESM has been roughly determined. Figure 5 shows the parameter description of the BEESM used in the optimization in this paper. Table 1 gives the initial design values of the main design parameters of BEESM and their ranges. The range of design parameters is mainly determined by the performance requirements and constraints of the structure. Taking into account the errors existing in the actual mass production process of the motor, Table 2 gives the possible noise of all design parameters. These noises have a significant impact on the robustness of the motor.

The performance indicators such as torque, torque ripple, and efficiency of BEESM are usually considered design goals. Since the thickness of the winding wire cannot be reflected in the FEM, it is generally believed that the diameter of the winding remains unchanged during the optimization process.

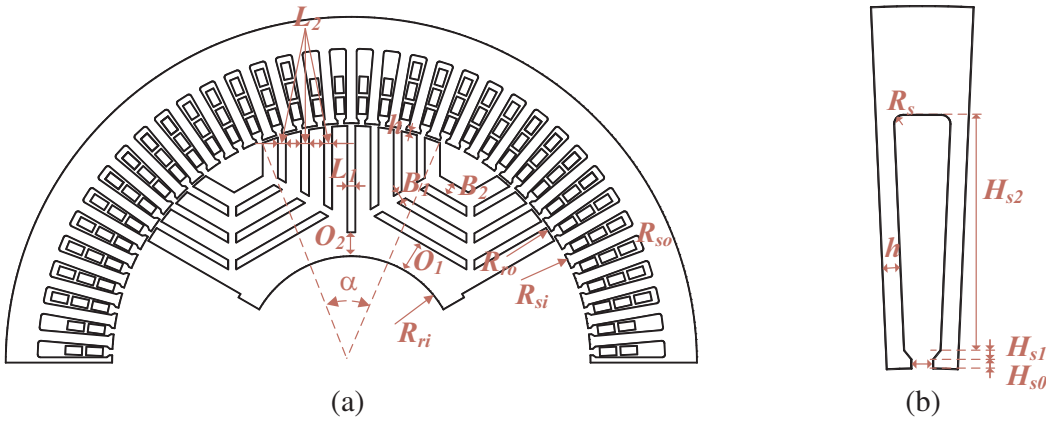

Figure 5. Parameter description of BEESM. (a) Main design parameters. (b) Design parameters of stator slots.

Table 1. Main design parameters of BEESM and their ranges.

	Parameter	Unit	Initial Design	Range
Stator	R_{so}	mm	65	-
	R_{si}	mm	45	-
	H_{s0}	mm	0.5	0.3–0.7
	H_{s1}	mm	0.5	0.3–0.7
	H_{s2}	mm	12.5	-
	B_{s0}	mm	1.2	-
	h	mm	2	-
	R_s	mm	0.5	-
	g	mm	0.5	
Rotor	R_{ro}	mm	44.5	-
	R_{ri}	mm	20	-
	α	deg	44	42–46
	O_1	mm	6	4–8
	O_2	mm	4.5	3–6
	B_1	mm	1.5	1–2
	B_2	mm	2.5	1.5–3.5
	L_1	mm	1.5	1–2
	L_2	mm	1.5	1–2

Keep the windings operating at the rated current density, so the copper loss of the motor is considered to be a fixed value. At this time, the biggest influence on motor loss is copper loss. At the same time, the rated torque of the motor is the main indicator of the performance of the motor. To ensure the smooth operation of the motor, the torque ripple of the motor also needs to be considered. Therefore, after comprehensive consideration, the rated torque, torque ripple, and iron loss of the motor are selected as the optimization targets, which are expressed as:

$$\min : \begin{cases} f_1(\mathbf{x}) = -T_e \\ f_2(\mathbf{x}) = P_{Fe} \\ f_3(\mathbf{x}) = T_r \end{cases} \tag{9}$$

And the motor also needs to satisfy certain constraints in the optimization process. These constraints

Table 2. The noises of design parameter.

	Parameter	Unit	Noises
Stator	H_{s0}	mm	$+/-0.1$
	H_{s1}	mm	$+/-0.1$
Rotor	α	deg	$+/-0.5$
	O_1	mm	$+/-0.1$
	O_2	mm	$+/-0.1$
	B_1	mm	$+/-0.1$
	B_2	mm	$+/-0.1$
	L_1	mm	$+/-0.1$
	L_2	mm	$+/-0.1$

are defined as:

$$\begin{cases} g_1(\mathbf{x}) = 0.7 - \eta \leq 0 \\ g_2(\mathbf{x}) = S_{slot} - 0.65 \leq 0 \\ g_3(\mathbf{x}) = J_C - 6 \leq 0 \end{cases} \tag{10}$$

5. SENSITIVITY ANALYSIS AND PARAMETER STRATIFICATION

To evaluate the correlation between different design parameters and optimization objectives, Kendall correlation analysis was performed on all design parameters. Figure 6 shows the Kendall rank coefficients for all design parameters. As shown, the correlations between different design parameters and design goals tend to be different. The sensitivity analysis results for different design parameters are shown in Figure 7, where Figure 7(a) is the local sensitivity of all design parameters. However, since the sensitivity value of α is too large, we separately represent other design parameters except for α in Figure 7(b). As can be seen from the figure, in addition to the higher sensitivity of α, B_1 also has a higher impact on the optimization objective. In contrast, design parameters such as B_2 and L_2 have less influence on the optimization objective. In contrast, design parameters such as B_2 and L_2 have less influence on the optimization objective. As shown in Table 3, all design parameters are divided into three subspaces after sensitivity analysis.

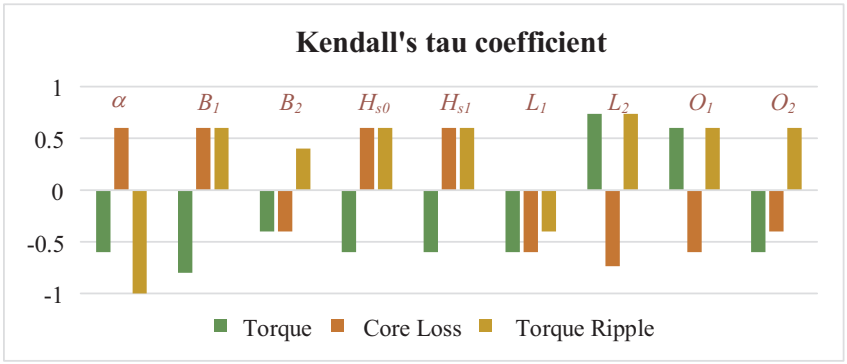

Figure 6. Kendall' tau coefficient.

After Kendall rank coefficient and local sensitivity analysis, all design parameters are divided into three subspaces. The highly sensitive parameter space ($\mathbf{S}_1$) contains parameters α and B_1; the sensitive parameter space ($\mathbf{S}_2$) contains parameters L_1, O_1, and O_2; the non-sensitive parameter space contains parameters B_2, H_{s0}, H_{s1}, and L_2.

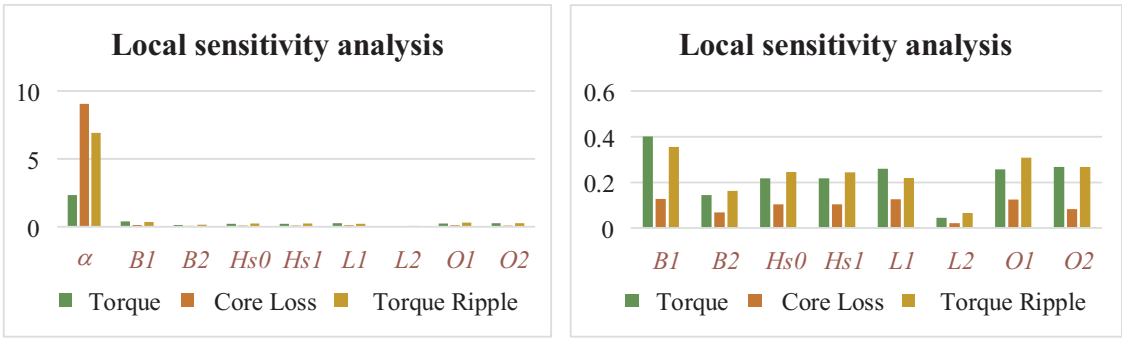

(a) (b)

Figure 7. Local sensitivity analysis results.

Table 3. Stratified results.

Subspace	Parameter
$\mathbf{S}_1$	α
	B_1
$\mathbf{S}_2$	L_1
	O_1
	O_2
$\mathbf{S}_3$	B_2
	H_{s0}
	H_{s1}
	L_2

6. RESULTS AND ANALYSIS

The optimization results of the first iterative process are shown in Figure 8. Among them, the peak points obtained by the improved climbing algorithm are marked as squares. All solution sets that lie on the Pareto front are marked with ordinal numbers. It can be seen from the figure that after the parameters in $\mathbf{S}_1$ are optimized, only two peak points are located on the Pareto front. Among them, the maximum torque point 1-1 reached 6.69 Nm, while the smallest torque point 1-2 was only 5.82 Nm, and the maximum and minimum torque ripple reached 104.37% and 62.71%, respectively. In

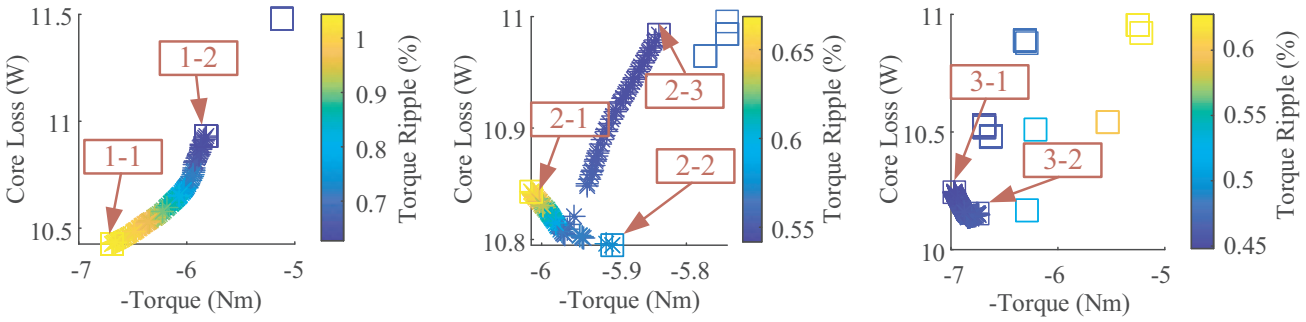

(a) (b) (c)

Figure 8. Results of the first iteration.

the optimization of $\mathbf{S}_2$, a total of 6 peak points are generated, of which only three are located in the Pareto front. In $\mathbf{S}_3$, only two peak points lie on the Pareto front and were selected for robustness analysis.

The robust optimization results of all design points in the first iteration process are shown in Figure 9. As shown in the figure, the performance of the motor changes to varying degrees after applying noise to the design point. As can be seen from the figure, for Point 1-1, when noise is applied to the design parameters, the torque changes by 0.65 Nm; the iron loss changes by 0.32 W; and the torque ripple changes by 13.21%. The performance changes of other design points after applying noise are shown in Table 4. After analysis by the method described in Section 3, Point 1-2 has better performance than Point 1-1, so it is input into the optimization of the next subspace. Likewise, in $\mathbf{S}_2$, Point 2-2 was selected because of its better performance in the robustness analysis results, and in $\mathbf{S}_3$, Point 3-2 was output as the final design result. The optimization results of each subspace are shown in Table 5.

After the first iteration is over, the optimization results are output to S1 for re-optimization. The second iteration process is shown in Figure 10 and Figure 11. After the second iterative process, judge whether the convergence condition is satisfied according to the method described in Section 2. After calculation, the error between the two is less than 5%, which satisfies the set convergence condition. Therefore, the optimization process ends, and the result of the second iteration process is output as the final result. The final optimization results are shown in Table 6.

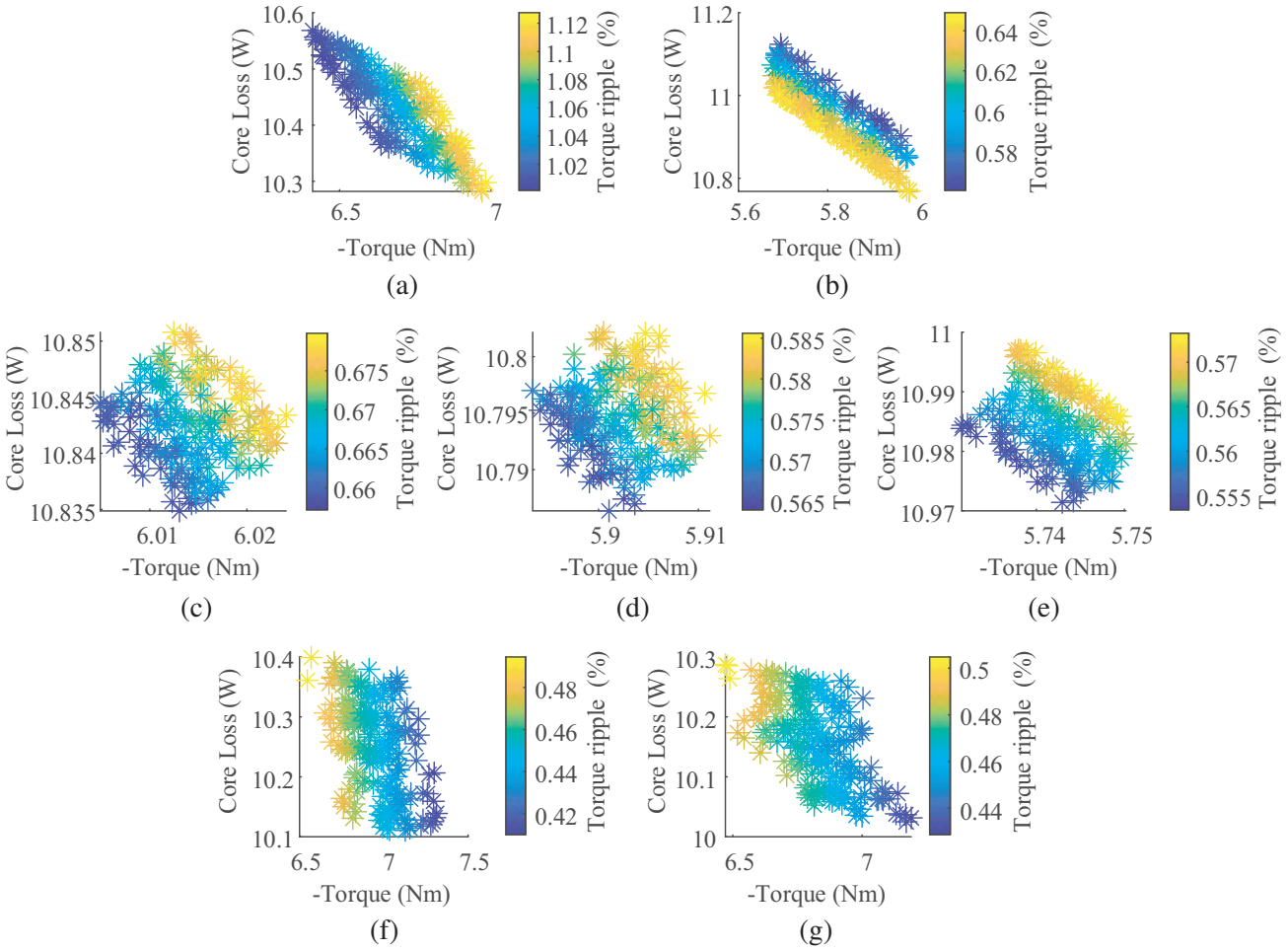

Figure 9. Results of the first iteration of robustness analysis for all design points. (a) Point 1-1. (b) Point 1-2. (c) Point 2-1. (d) Point 2-2. (e) Point 2-3. (f) Point 3-1. (g) Point 3-2.

Table 4. Performance change after applying noise at all design points in the first iteration.

	Point	Δ T(Nm)	ΔP_{Fe} (W)	ΔT_r (%)
Space1	1-1	0.65	0.32	13.21
	1-2	0.30	0.30	9.36
Space2	2-1	0.02	0.02	2.28
	2-2	0.02	0.02	2.16
	2-3	0.02	0.03	2.57
Space3	3-1	0.73	0.25	7.77
	3-2	0.71	0.24	7.54

Table 5. Optimization results of the first iteration process.

Parameter	Unit	Initial	S1	S2	S3
α	deg	44.00	46.00	46.00	46.00
B_1	mm	1.50	1.03	1.03	1.03
L_1	mm	1.50	1.50	2.00	2.00
O_1	mm	6.00	6.00	8.00	8.00
O_2	mm	4.50	4.50	6.00	6.00
B_2	mm	2.50	2.50	2.50	3.38
H_{s0}	mm	0.50	0.50	0.50	0.30
H_{s1}	mm	0.50	0.50	0.50	0.37
L_2	mm	1.50	1.50	1.50	2.00
Torque	Nm	5.36	5.82	5.90	6.75
CoreLoss	W	11.21	10.93	10.79	10.15
Ripple	%	79.86	62.71	57.49	46.17

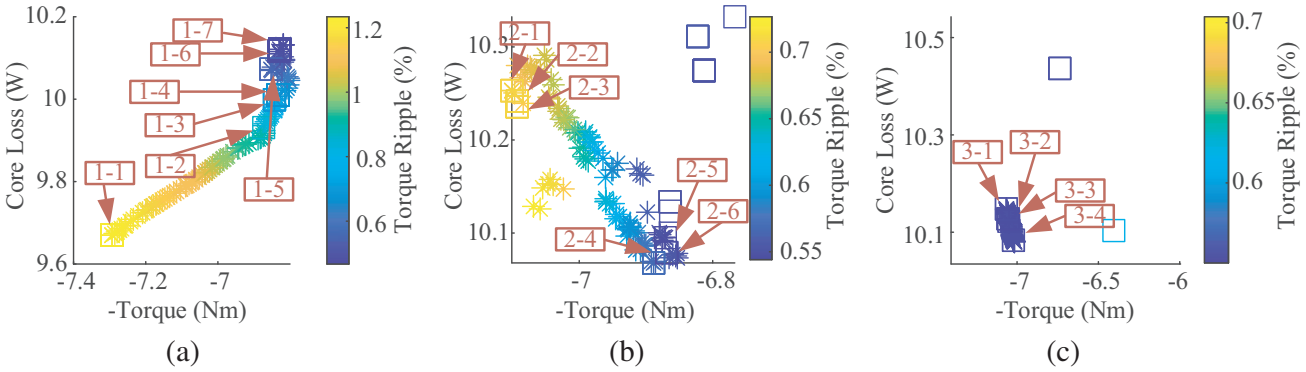

Figure 10. Optimization results for the second iteration.

Figures 12–14 show the comparison of the main performance of the motors before and after optimization. To verify the robustness of the initial and optimal designs, random noise was imposed on the two motor models. As shown in Figure 12, after applying noise, the torque at the initial design point has a change of 0.22 Nm, while the torque change at the optimal design point is only 0.04 Nm. The loss change at the initial design point is 0.15 W, and the torque ripple change is 16.73%, while the loss change and torque ripple change at the optimum design point are 0.09 W and 11.84%, respectively.

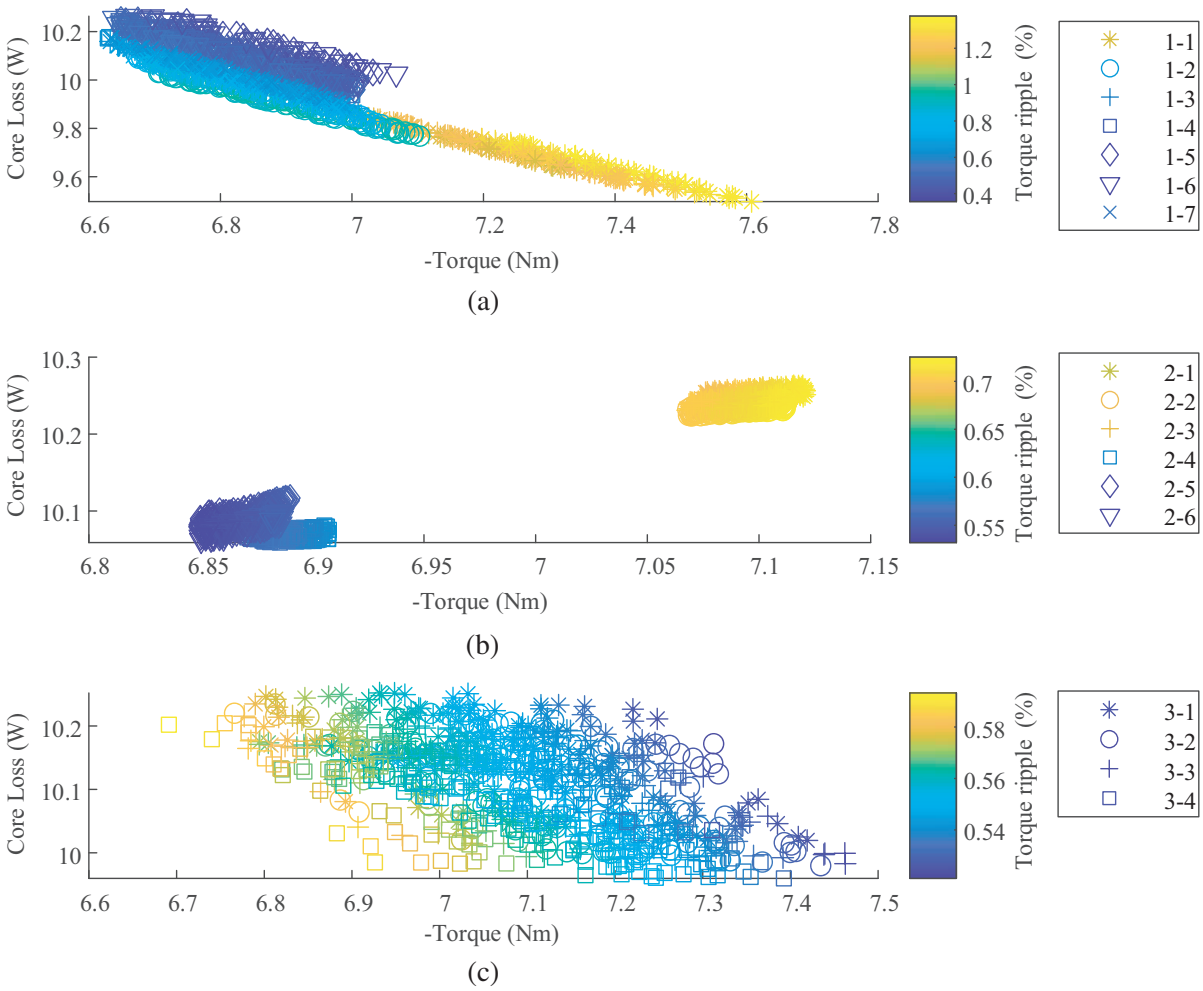

Figure 11. Robust optimization results for all design points in the second iteration. (a) $\mathbf{S}_1$. (b) $\mathbf{S}_2$. (c) $\mathbf{S}_3$.

Table 6. Final optimization result.

Parameter	Unit	Initial	Optimal
α	deg	44.00	45.21
B_1	mm	1.50	1
L_1	mm	1.50	1.79
O_1	mm	6.00	8
O_2	mm	4.50	5.69
B_2	mm	2.50	1.5
H_{s0}	mm	0.50	0.3
H_{s1}	mm	0.50	0.3
L_2	mm	1.50	2
Torque	Nm	5.36	7.06
Core-Loss	W	11.21	10.13
Ripple	%	79.86	55.00

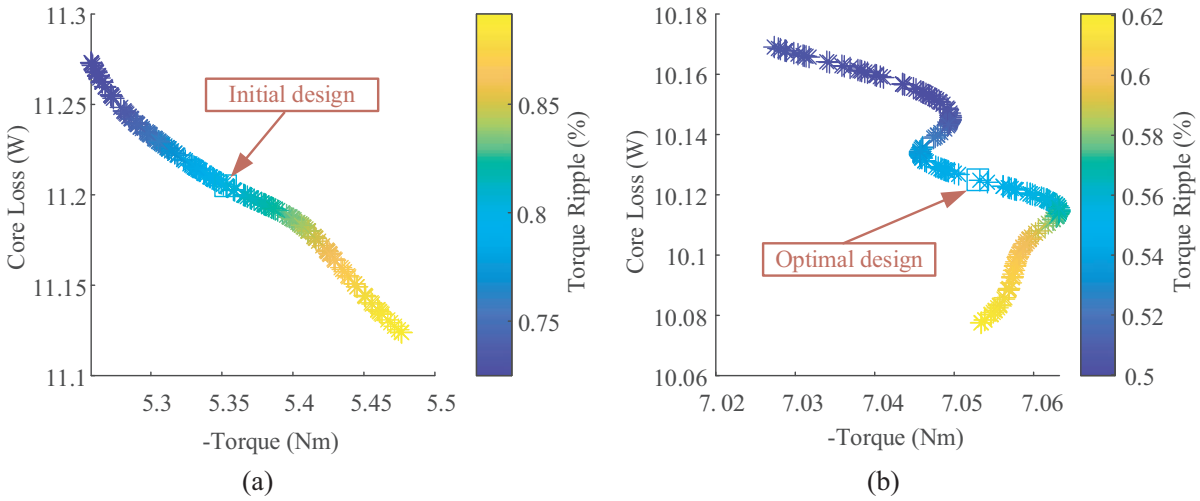

Figure 12. Comparison of motor robustness before and after optimization.

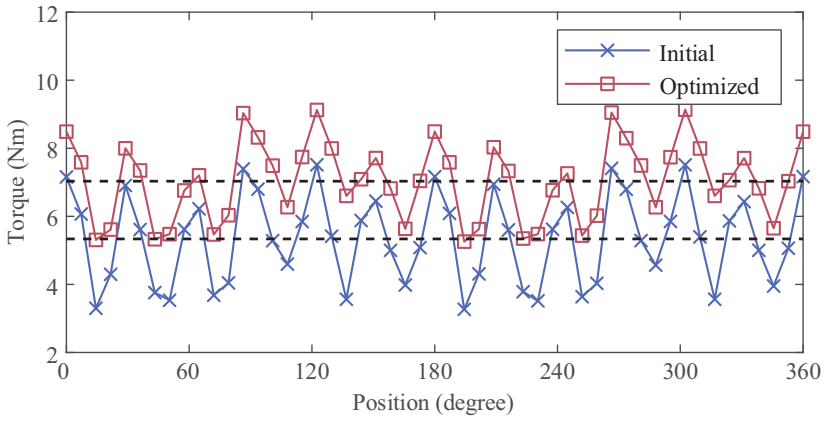

Figure 13. Comparison of motor torque before and after optimization.

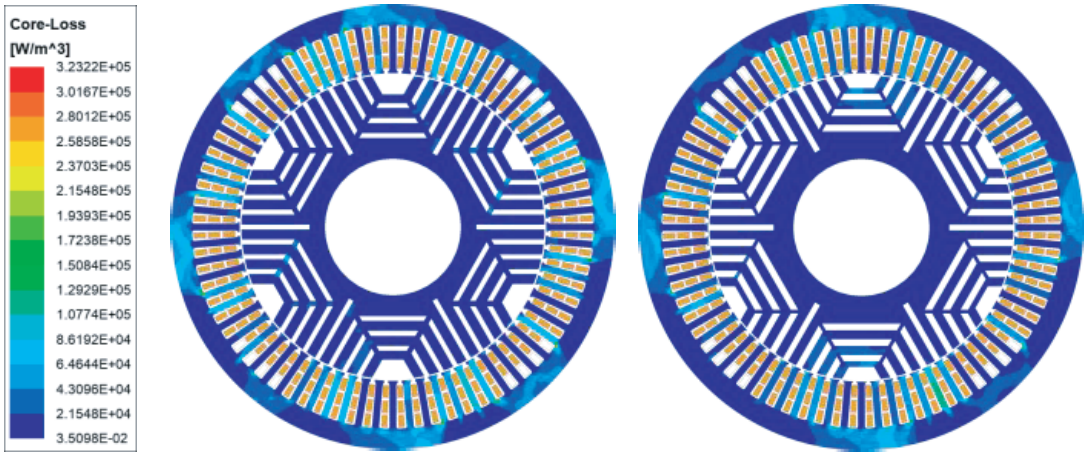

Figure 14. Comparison of motor losses before and after optimization.

For all optimization objectives, the motor designed with optimal robustness has better performance than the initial design.

The torque comparison between the initial design and the optimal design is obtained through the FEM experiment, and the torque curve is shown in Figure 13. As can be seen from the figure, the optimized motor has more torque and less torque ripple. Figure 14 shows the distributions of motor losses before and after optimization. It can be seen from the figure that in the optimized motor loss distribution diagram, the area of the high loss area is smaller than that of the initially designed motor, so the optimized motor has a smaller iron loss than the initially designed motor.

7. CONCLUSION

In this paper, a robust multi-objective optimization design method of BEESM based on an improved climbing algorithm is proposed. After the initial design of the motor and the establishment of the mathematical model of the optimization problem, all the design parameters are divided into three subspaces according to the sensitivity by the sensitivity analysis method combined with Kendall's rank coefficient. The optimization process of the motor will be carried out sequentially in these three subspaces. By dividing all parameters into three subspaces, the cost of FEM computation is greatly reduced. At the same time, through sensitivity analysis, more computing resources can be allocated to highly sensitive parameters, which can improve the accuracy and efficiency of optimization while reducing computing consumption. The screening problem of Pareto frontier solutions is solved by an improved climbing algorithm. The candidate points to be optimized are screened through the improved climbing algorithm, and only the candidate points located on the Pareto frontier will be optimized, which ensuring the high performance of the candidate points. Based on the noise problems that may occur in actual production and processing, the candidate points are robustly analyzed, and the optimal design is screened out. The final optimization results and the initial design were analyzed and compared by FEM. The results show that the robust optimization design method proposed in this paper reduces the computational cost and improves the optimization efficiency based on improving motor performance.

ACKNOWLEDGMENT

This work was supported by the National Natural Science Foundation of China under Project 52002155.

REFERENCES

1. Zhang, F. G., G. L. Jia, Y. Zheng, and T. Guan, "Analysis and experimental study of brushless electrically-excited synchronous generator with hybrid rotor," *2015 IEEE International Conference on Applied Superconductivity and Electromagnetic Devices (ASEMD)*, 332–333, Nov. 2015.
2. Pallantla, M., P. Kumar, and N. Mohan, "Comparison and evaluation of the different brushless excitation topologies for synchronous machines — A literature survey," *2020 IEEE International Conference on Power Electronics, Smart Grid and Renewable Energy (PESGRE2020)*, 1–6, Jan. 2020.
3. Berweiler, B. and B. Ponick, "Current and average temperature calculation for electrically excited synchronous machines in case of contactless energy supply," *2020 International Conference on Electrical Machines (ICEM)*, Vol. 1, 1730–1735, Aug. 2020.
4. Hsieh, M.-F., Y.-H. Chang, and D. G. Dorrell, "Design and analysis of brushless doubly fed reluctance machine for renewable energy applications," *IEEE Trans. Magn.*, Vol. 52, No. 7, 1–5, Jul. 2016.
5. Zhang, F., H. Wang, G. Jia, D. Ma, and M. G. Jovanovic, "Effects of design parameters on performance of brushless electrically excited synchronous reluctance generator," *IEEE Trans. Ind. Electron.*, Vol. 65, No. 11, 9179–9189, Nov. 2018.
6. Zhang, F., J. Xu, G. Jia, and S. Jin, "Electromagnetic design and dynamic performance study of electrically excited brushless synchronous motor," *2013 International Conference on Electrical Machines and Systems (ICEMS)*, 699–702, Oct. 2013.

7. Chakraborty, C. and Y. T. Rao, "Performance of brushless induction excited synchronous generator," *IEEE J. Emerg. Sel. Top. Power Electron.*, Vol. 7, No. 4, 2571–2582, Dec. 2019.
8. Gorginpour, H., H. Oraee, and R. A. McMahon, "Electromagnetic-thermal design optimization of the brushless doubly fed induction generator," *IEEE Trans. Ind. Electron.*, Vol. 61, No. 4, 1710–1721, Apr. 2014.
9. Hussain, A., S. Atiq, and B. Kwon, "Optimal design and experimental verification of wound rotor synchronous machine using subharmonic excitation for brushless operation," *Energies*, Vol. 11, No. 3, Art. No. 3, Mar. 2018.
10. Sun, L., X. Gao, F. Yao, Q. An, and T. Lipo, "A new type of harmonic current excited brushless synchronous machine based on an open winding pattern," *2014 IEEE Energy Conversion Congress and Exposition (ECCE)*, 2366–2373, Sep. 2014.
11. Usinin, Yu. S., M. A. Grigorjev, K. M. Vinogradov, and S. P. Gladyshev, "New brushless synchronous machine for vehicle application," *SAE Trans.*, Vol. 116, 270–276, 2007.
12. Zhang, F., G. Jia, Y. Zhao, Z. Yang, W. Cao, and J. L. Kirtley, "Simulation and experimental analysis of a brushless electrically excited synchronous machine with a hybrid rotor," *IEEE Trans. Magn.*, Vol. 51, No. 12, 1–7, Dec. 2015.
13. Long, Q., Z. Zhou, X. Lin, and J. Liao, "Investigation of a novel brushless electrically excited synchronous machine with arc-shaped rotor structure," *Energy Rep.*, Vol. 6, 608–617, Dec. 2020.
14. Ali, Q., T. A. Lipo, and B.-I. Kwon, "Design and analysis of a novel brushless wound rotor synchronous machine," *IEEE Trans. Magn.*, Vol. 51, No. 11, 1–4, Nov. 2015.
15. Yao, F., Q. An, L. Sun, and T. A. Lipo, "Performance investigation of a brushless synchronous machine with additional harmonic field windings," *IEEE Trans. Ind. Electron.*, Vol. 63, No. 11, 6756–6766, Nov. 2016.
16. Spielmann, H. and H. E. Friedrich, "Method to optimize NVH-behaviour of a brushless electrically excited synchronous machine," *2018 Thirteenth International Conference on Ecological Vehicles and Renewable Energies (EVER)*, 1–8, Apr. 2018.
17. Sun, X., Z. Shi, G. Lei, Y. Guo, and J. Zhu, "Analysis and design optimization of a permanent magnet synchronous motor for a campus patrol electric vehicle," *IEEE Trans. Veh. Technol.*, Vol. 68, No. 11, 10535–10544, Nov. 2019.
18. Salimi, A. and D. A. Lowther, "On the role of robustness in multi-objective robust optimization: Application to an IPM motor design problem," *IEEE Trans. Magn.*, Vol. 52, No. 3, 1–4, Mar. 2016.
19. Sun, X., N. Xu, and M. Yao, "Sequential subspace optimization design of a dual three-phase permanent magnet synchronous hub motor based on NSGA III," *IEEE Trans. Transp. Electrification*, 1–1, 2022.
20. Shi, Z., X. Sun, G. Lei, X. Tian, Y. Guo, and J. Zhu, "Multiobjective optimization of a five-phase bearingless permanent magnet motor considering winding area," *IEEE ASME Trans. Mechatron.*, 1–10, 2021.
21. Ma, B., G. Lei, C. Liu, J. Zhu, and Y. Guo, "Robust tolerance design optimization of a PM claw pole motor with soft magnetic composite cores," *IEEE Trans. Magn.*, Vol. 54, No. 3, 1–4, Mar. 2018.
22. Sun, X., Z. Shi, and J. Zhu, "Multiobjective design optimization of an IPMSM for EVs based on fuzzy method and sequential taguchi method," *IEEE Trans. Ind. Electron.*, Vol. 68, No. 11, 10592–10600, 2021.
23. Liu, G., Y. Wang, Q. Chen, G. Xu, and C. Song, "Multiobjective deterministic and robust optimization design of a new spoke-type permanent magnet machine for the improvement of torque performance," *IEEE Trans. Ind. Electron.*, Vol. 67, No. 12, 10202–10212, 2020.
24. Kim, K.-S., K.-T. Jung, J.-M. Kim, J.-P. Hong, and S.-I. Kim, "Taguchi robust optimum design for reducing the cogging torque of EPS motors considering magnetic unbalance caused by manufacturing tolerances of PM," *IET Electr. Power Appl.*, Vol. 10, No. 9, 909–915, 2016.

25. Sun, X., Z. Shi, Y. Cai, G. Lei, Y. Guo, and J. Zhu, "Driving-cycle-oriented design optimization of a permanent magnet hub motor drive system for a four-wheel-drive electric vehicle," *IEEE Trans. Transp. Electrification*, Vol. 6, No. 3, 1115–1125, Sep. 2020.
26. Lee, J.-G., N.-W. Hwang, H. Ryu, H.-K. Jung, and D.-K. Woo, "Robust optimization approach applied to permanent magnet synchronous motor," *IEEE Trans. Magn.*, Vol. 53, No. 6, 1–4, Jun. 2017.
27. Diao, K., X. Sun, G. Bramerdorfer, Y. Cai, G. Lei, and L. Chen, "Design optimization of switched reluctance machines for performance and reliability enhancements: A review," *Renew. Sustain. Energy Rev.*, Vol. 168, 112785, Oct. 2022.
28. Jin, Z., X. Sun, L. Chen, and Z. Yang, "Robust multi-objective optimization of a 3-pole active magnetic bearing based on combined curves with climbing algorithm," *IEEE Trans. Ind. Electron.*, Vol. 69, No. 6, 5491–5501, Jun. 2022.
29. Almansa Malagoli, J., J. R. Camacho, M. Valencia Ferreira da Luz, J. H. Inacio Ferreira, and A. Maximiano Sobrinho, "Design of three-phase induction machine using differential evolution algorithm," *IEEE Lat. Am. Trans.*, Vol. 13, No. 7, 2202–2208, Jul. 2015.
30. Jolly, L., M. A. Jabbar, and L. Qinghua, "Design optimization of permanent magnet motors using response surface methodology and genetic algorithms," *IEEE Trans. Magn.*, Vol. 41, No. 10, 3928–3930, 2005.
31. Lee, J. H., J.-W. Kim, J.-Y. Song, D.-W. Kim, Y.-J. Kim, and S.-Y. Jung, "Distance-based intelligent particle swarm optimization for optimal design of permanent magnet synchronous machine," *IEEE Trans. Magn.*, Vol. 53, No. 6, 1–4, Jun. 2017.
32. Sim, D.-J., D.-H. Cho, J.-S. Chun, H.-K. Jung, and T.-K. Chung, "Efficiency optimization of interior permanent magnet synchronous motor using genetic algorithms," *IEEE Trans. Magn.*, Vol. 33, No. 2, 1880–1883, Mar. 1997.
33. Bokose, F. L., L. Vandevelde, and J. A. A. Melkebeek, "Sequential approximate multiobjective optimisation of switched reluctance motor design using surrogate models and nongradient local search algorithm," *IEE Proc. — Sci. Meas. Technol.*, Vol. 151, No. 6, 471–475, Nov. 2004.
34. Xia, B., M.-T. Pham, Y. Zhang, and C.-S. Koh, "A global optimization algorithm for electromagnetic devices by combining adaptive taylor kriging and particle swarm optimization," *IEEE Trans. Magn.*, Vol. 49, No. 5, 2061–2064, 2013.
35. Sun, X., Z. Shi, G. Lei, Y. Guo, and J. Zhu, "Multi-objective design optimization of an IPMSM based on multilevel strategy," *IEEE Trans. Ind. Electron.*, Vol. 68, No. 1, 139–148, Jan. 2021.
36. Sun, X., Z. Shi, and J. Zhu, "Multi-objective design optimization of an IPMSM for EVs based on fuzzy method and sequential taguchi method," *IEEE Trans. Ind. Electron.*, Vol. 68, No. 11, 10592–10600, 2021.
37. Si, J., S. Zhao, H. Feng, R. Cao, and Y. Hu, "Multi-objective optimization of surface-mounted and interior permanent magnet synchronous motor based on Taguchi method and response surface method," *Chin. J. Electr. Eng.*, Vol. 4, No. 1, 67–73, Mar. 2018.
38. Shi, Z. and X. Sun, "Robust design optimization of a five-phase PM hub motor for fault-tolerant operation based on taguchi method," *IEEE Trans. Energy Convers.*, Vol. 35, No. 4, 9, 2020.
39. Croux, C. and C. Dehon, "Influence functions of the Spearman and Kendall correlation measures," *Stat. Methods Appl.*, Vol. 19, No. 4, 497–515, Nov. 2010.
40. Lebensztajn, L., C. A. R. Marretto, M. C. Costa, and J.-L. Coulomb, "Kriging: A useful tool for electromagnetic device optimization," *IEEE Trans. Magn.*, Vol. 40, No. 2, 1196–1199, Mar. 2004.
41. Deb, K., A. Pratap, S. Agarwal, and T. Meyarivan, "A fast and elitist multiobjective genetic algorithm: NSGA-II," *IEEE Trans. Evol. Comput.*, Vol. 6, No. 2, 182–197, Apr. 2002.
42. Shi, Z., X. Sun, G. Lei, Z. Yang, Y. Guo, and J. Zhu, "Analysis and optimization of radial force of permanent-magnet synchronous hub motors," *IEEE Trans. Magn.*, Vol. 56, No. 2, 1–4, 2020.
43. Sun, Q., W. Zhang, and Q. Wang, "Fundamental design and analysis of a novel bipolar transverse-flux motor with stator permanent-magnet excitation," *Chin. J. Electr. Eng.*, Vol. 4, No. 1, 60–66, Mar. 2018.